Supplement of Biogeosciences, 18, 2289–2300, 2021
https://doi.org/10.5194/bg-18-2289-2021-supplement

Biogeosciences Open Access EGU

Supplement of

Lignin oxidation products in soil, dripwater and speleothems from four different sites in New Zealand

Inken Heidke et al.

Correspondence to: Thorsten Hoffmann (t.hoffmann@uni-mainz.de)

S1 Analytical methods

For the soil samples, the LC-MS analysis of the lignin oxidation products was performed as described in Heidke et al. (2018) using a 50 mm pentafluorophenyl (PFP) column (Hypersil GOLD PFP, 50 mm $\times$ 2.1 mm with 1.9 μm particle size by Thermo Fisher Scientific). For the dripwater and flowstone samples, a 100 mm PFP column (Aquity UPLC CSH Fluoro-Phenyl, 100 mm $\times$ 2.1 mm with 1.7 μm particle size by Waters) was used for the separation of the LOPs. The gradient for this column started with 5% eluent B (98% acetonitrile, 2% H_2O) and 95% eluent A (98% H_2O, 2% acetonitrile and 0.4 $\mu L \cdot L^{-1}$ formic acid). Eluent B increased to 10% until 0.5 min, was held at this stage until 5.0 min, increased to 15% until 6.0 min and to 50% until 7.5 min. Then, a cleaning step at 99% B was run from 7.5 to 9.5 min, and finally, the initial eluent mixture with 5% B was reequilibrated from 9.5 to 11.0 min. The flow was set to 500 $\mu L \cdot min^{-1}$ and the column oven was heated to 40 °C.

The electrospray ionisation source (ESI) was operated in negative mode, so that deprotonated molecular ions $[M\text{-}H]^-$ were formed. The spray voltage was -3.5 kV, the ESI probe was heated to 150 °C to improve the evaporation of the aqueous solvent, the capillary temperature was 320 °C, the sheath gas pressure was 60 psi and the auxiliary gas pressure was 20 psi.

The mass spectrometer(Q Exactive Orbitrap high-resolution mass spectrometer by Thermo Fisher Scientific) was operated in full scan mode with a resolution of 70 000 and a scan range of *m/z* 80–500. At the respective retention time windows, the full scan mode was alternated with a targeted MS^2-mode with a resolution of 17 500 to identify the LOPs by their specific daughter ions (Heidke et al., 2018). For the MS^2-mode (i.e., *parallel reaction monitoring mode* in the software *XCalibur*, provided by Thermo Fisher Scientific), higher-energy collisional dissociation (HCD) was used with 35% normalized collision energy (NCE) for all analytes.

S2 Description of the cave sites

Soils have been described to the most appropriate soil order following the New Zealand Soil Classification (NZSC, Hewitt (2010)). A brief description of the vegetation and soils of the four different cave sites is given in the following paragraphs.

Waipuna Cave, Waitomo (Fig. S1, situated at S 38.3114722°, E 175.0206389°), is covered by a lush podocarp forest with a dense undergrowth of shrubs, ferns and tree-ferns. Soils in the locality are deep (> 1m) typic orthic allophanic (LO) being developed on extensive North Island rhyolitic volcanic ash deposits. These soils are exceptionally well drained and water typically reaches the cave on the timescale of days to a few weeks following rainfall events (Nava-Fernandez et al., 2020).

Figure S1. Vegetation (a) and soils (b) of Waipuna Cave, Waitomo, North Island.

Hodges Creek Cave, Mt Arthur Tablelands, (Fig. S2, situated at S 41.171270°, E 172.685941°) is developed within an Oligocene limestone remnant that has been heavily weathered and incised by deep grykes within which extensive litter organic (LO) soils have accumulated, which in places transition to orthic gley (GO) due to water logging leading to iron reduction, with characteristic iron mottles and concretions being found at depth (right hand picture). On the more gentle slopes, mature beech forest and well-drained orthic podzol (ZO) soils are typical with a deep brown O horizon and a weak sub-soil composed of bleached clays and weathered limestone.

The steep beech-covered slopes of Mt Arthur have only a thin orthic podzol (ZO) soil (Fig. S3, Nettlebed Cave situated at S 41.2104589°, E 172.7394572°). Typically they are well-drained with a weak, bleached sub-soil due to the abundant, acidic leaf litter.

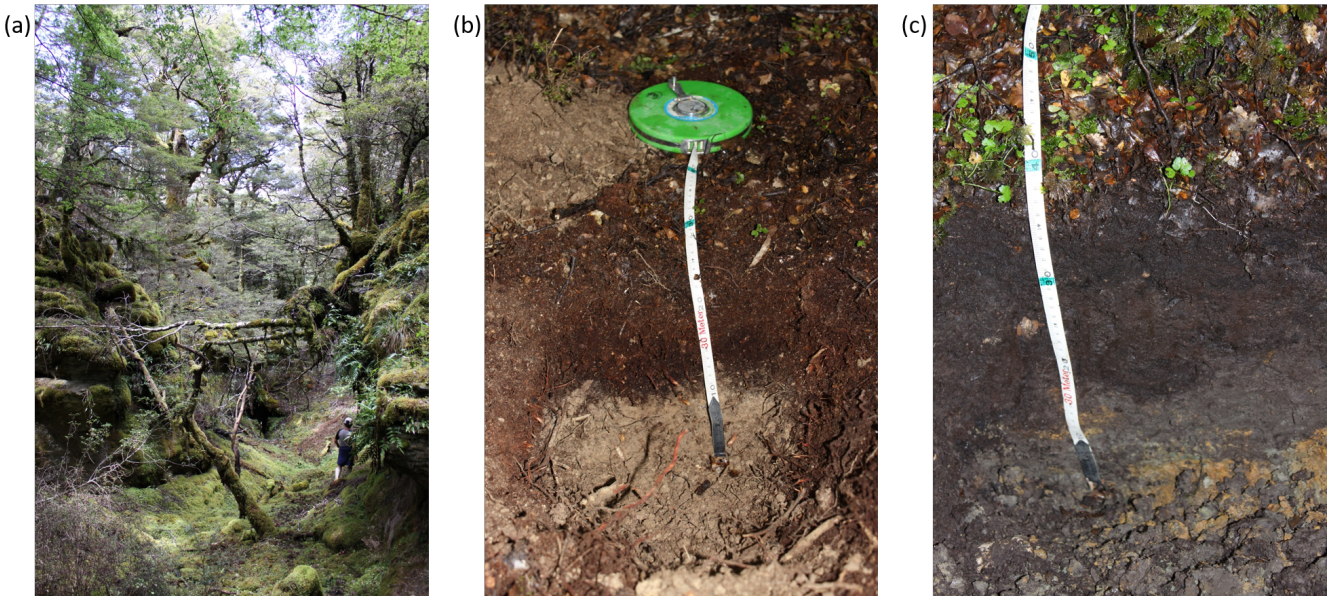

Figure S2. Vegetation (a) and soils (b) and (c) of Hodges Creek Cave, Mt Arthur Tablelands, Kahurangi National Park, South Island.

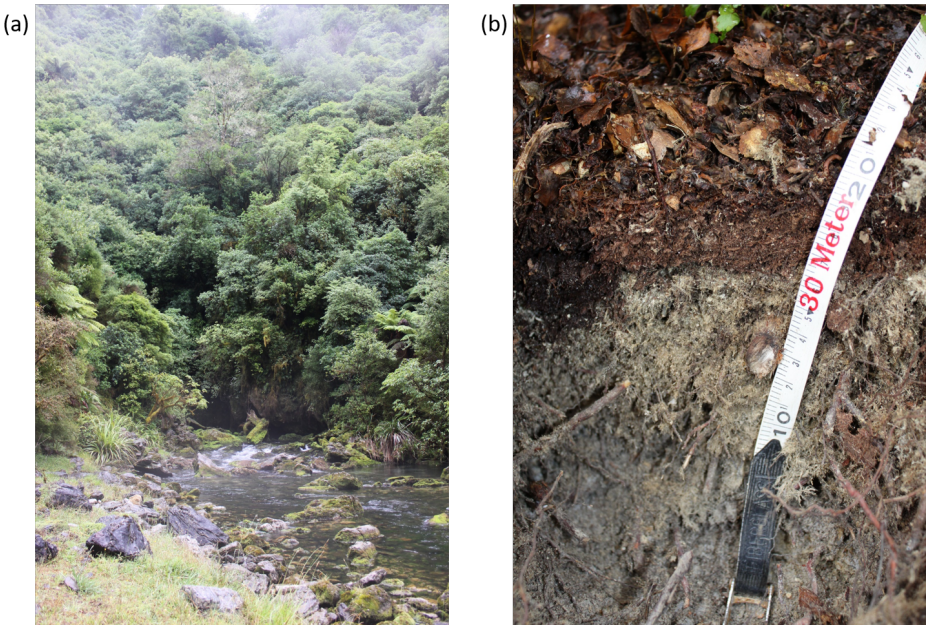

Figure S3. Vegetation (a) and soils (b) of Nettlebed Cave, Mt Arthur, Kahurangi National Park, South Island.

The Mt Luxmore caves (Fig. S4, Daves cave situated at S 45.3894900°, E 167.6153448°) reside above the tree line under a thick ground cover of tussock and other native alpine plants. Cold and wet conditions promote water-logging and peaty organic rich soils have developed. Soils were found to have light brown A horizons beginning at around 20 cm with characteristic iron staining indicating iron reduction and oxidation within the soil profile.

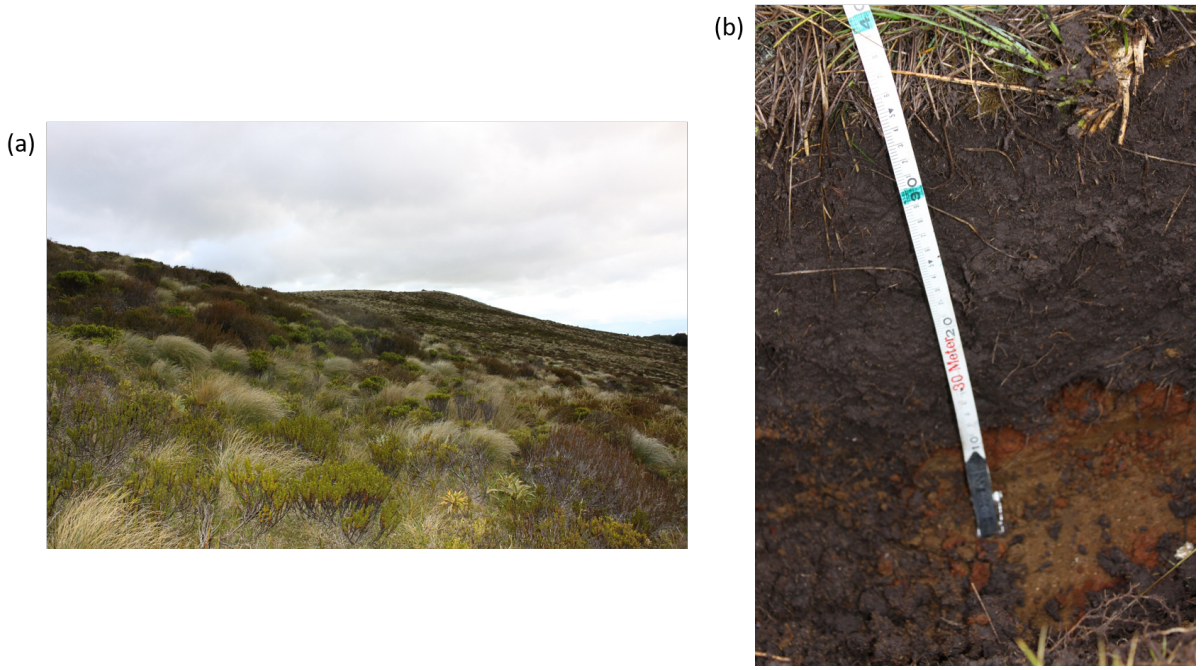

Figure S4. Vegetation (a) and soils (b) of Dave's Cave, Mt Luxmore, Fiordland National Park, South Island.

S3 Photographs of the flowstone samples

In Figure S5, photographs of the flowstone cores from WP, HC, NB and DC are shown. The samples analyzed in this study are marked in red.

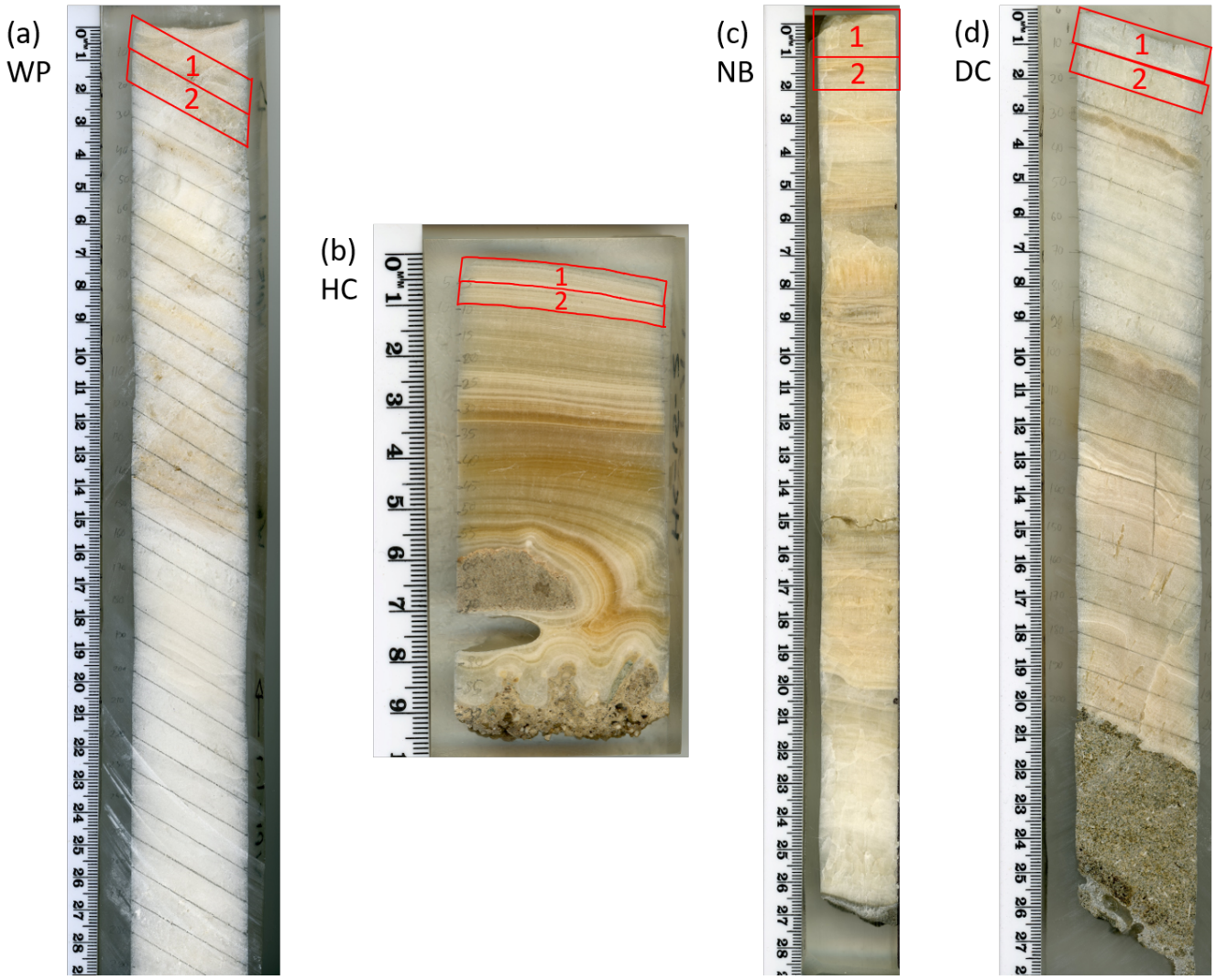

Figure S5. Photographs of the flowstone cores from (a) Waipuna Cave (WP), (b) Hodges Creek Cave (HC), (c) Nettlebed Cave (NB), and (d) Daves Cave (DC). The samples analyzed in this study are marked in red.

S4 ^{230}Th/U-dating of flowstone cores

Photographs of the flowstone slabs with the trenches drilled for ^{230}Th/U-dating are shown in Figure S6. All relevant data concerning the ^{230}Th/U-dating of the flowstone cores are shown in Table S1. Age-depth models of the four flowstone cores are shown in Figure S7.

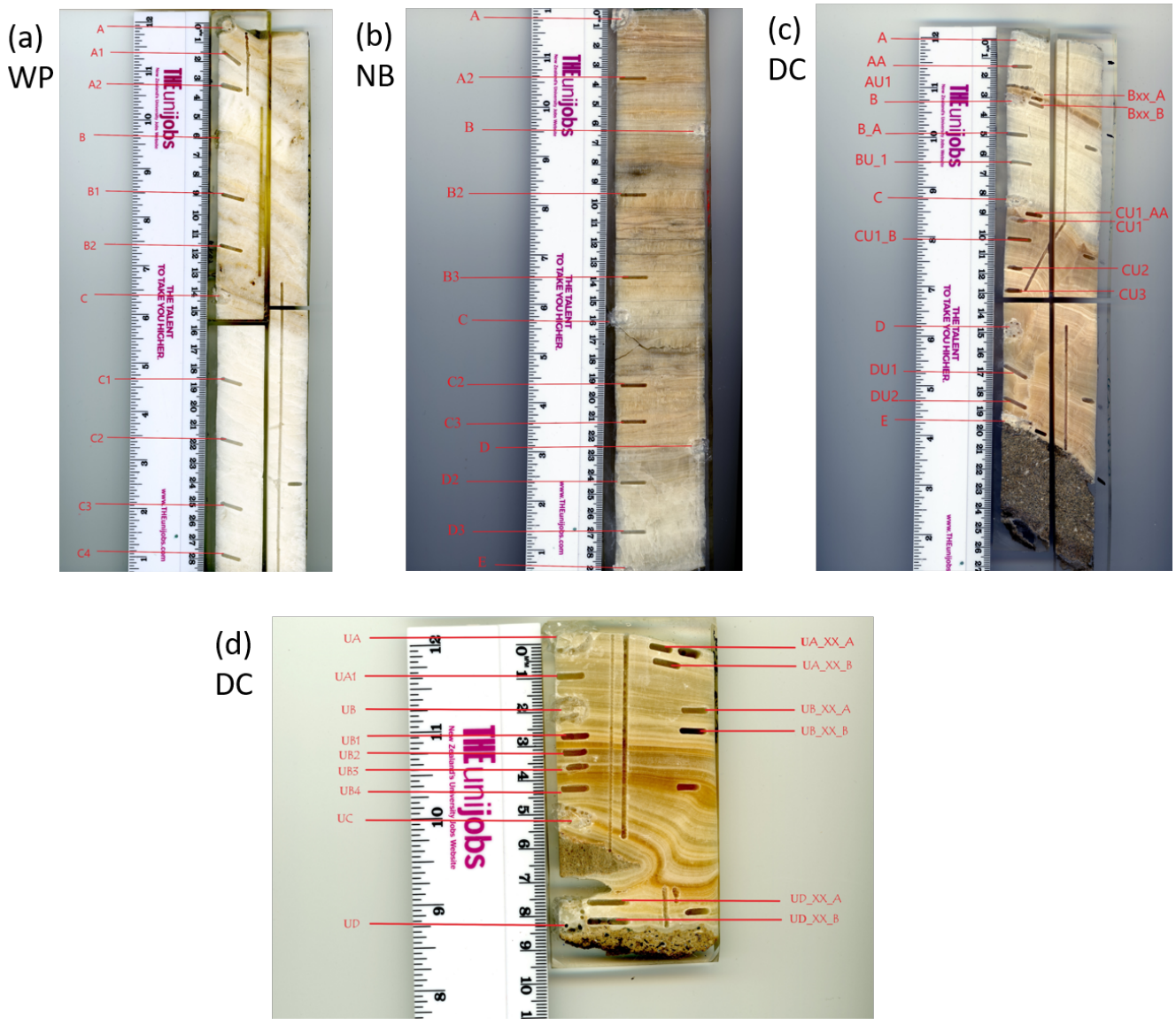

Figure S6. Photographs of the flowstone slabs with the trenches drilled for ^{230}Th/U-dating.

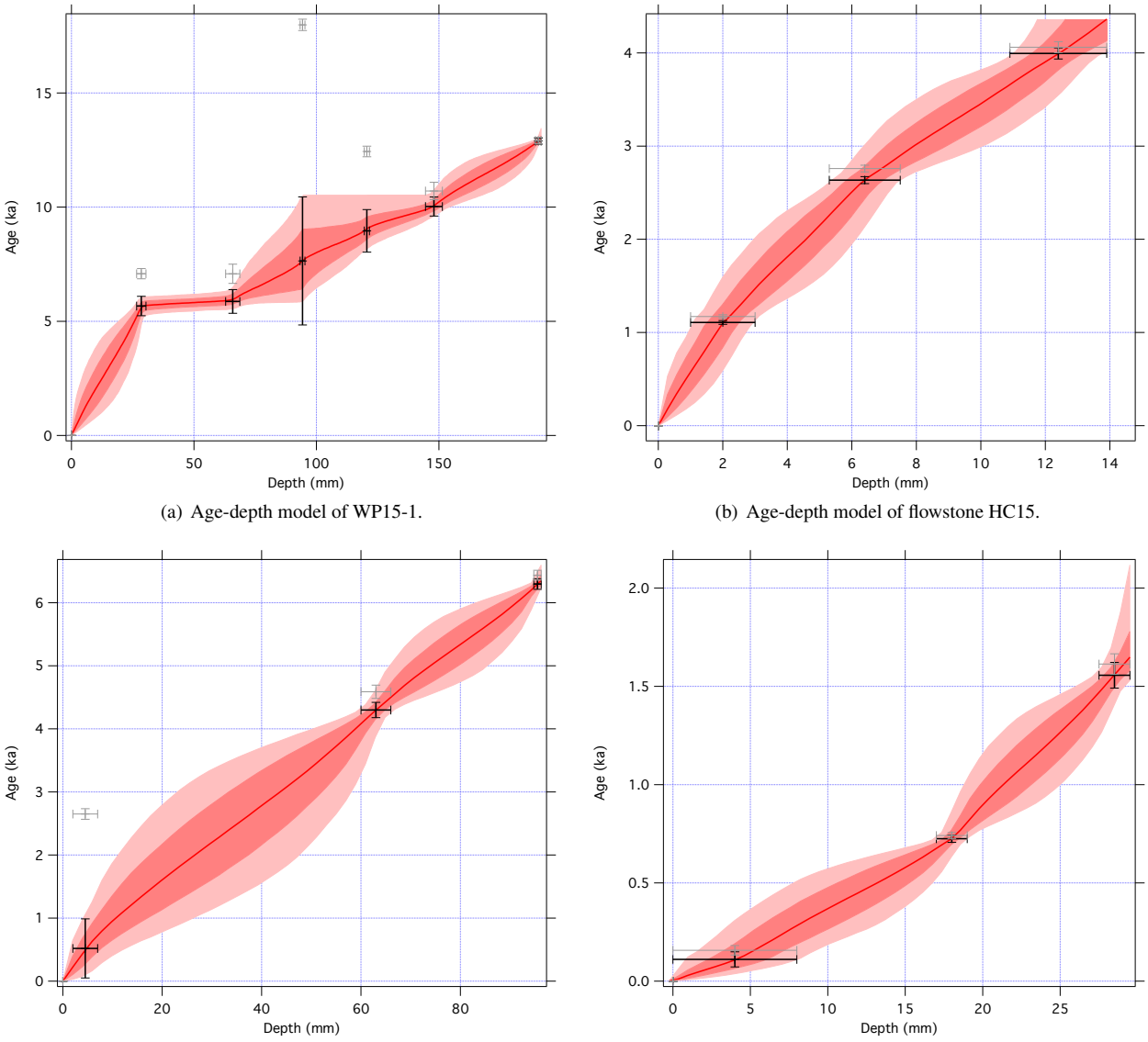

(a) Age-depth model of WP15-1.

(b) Age-depth model of flowstone HC15.

(c) Age-depth model of flowstone NB15.

(d) Age-depth model of flowstone DC15.

Figure S7. Age-depth models of the four flowstone cores.

Table S1. ^{230}Th/U-dating of the flowstone cores.

Sample	Lab Number	Depth in mm	U in ngg^{-1}	[^{230}Th/^{238}U]^{a}	[^{234}U/^{238}U]^{a}	[^{232}Th/^{238}U]	[^{230}Th/^{232}Th]	[^{230}Th/^{232}Th]$^{d}_{i}$	Age in ka^{b}	[^{234}U/^{238}U]$^{c}_{i}$
HC15 - Mt Arthur										
HC15_2_UA_XX_A	UME190501-621	2.0(1.0)	157	0.01816(32)	1.7017(27)	0.001144(23)	16	0.860(0.086)	1.109(0.021)	1.7039(27)
HC15_2_UA_XX_B	UME190501-628	6.4(1.1)	110	0.03921(53)	1.5661(26)	0.002090(42)	19	0.860(0.086)	2.635(0.039)	1.5703(26)
HC15 2 U-A-1	UMD170809-250	12.4(1.5)	120	0.05671(76)	1.5479(43)	0.001093(24)	52	0.860(0.086)	3.995(0.060)	1.5541(43)
WP15 - Waitomo										
*WP15 1.1 A	UMD170809-407	3.8(3.8)	13	0.1163(37)	1.2226(46)	0.08245(23)	1.4	0.71(0.18)	5.5(1.4)	1.2261(47)
WP15_1.1_UA_1	UME190820-307	17.0(1.0)	22	0.0758(23)	1.2027(52)	0.02191(44)	3.5	0.71(0.18)	5.67(0.43)	1.2059(52)
WP15 1.1 B	UMD170809-409	60.0(4.0)	16	0.0803(46)	1.2744(61)	0.01984(09)	4.0	0.71(0.18)	5.87(0.52)	1.2789(62)
DC15 - Mt Luxmore										
DC15 1.1A	UMD160610-423	4.0(4.0)	17	0.00200(31)	1.3917(42)	0.0007748(30)	2.6	0.75(0.50)	0.111(0.038)	1.3918(42)
DC15_1.1_AA	UME190501-657	18.0(1.0)	147	0.00976(18)	1.4468(21)	0.0002747(55)	36	0.75(0.50)	0.726(0.018)	1.4477(21)
DC15 1.1 UA1	UMD170809-343	28.5(1.0)	161	0.02195(70)	1.4894(42)	0.0010429(30)	21	0.75(0.50)	1.557(0.064)	1.4915(43)
NB15 - Mt Arthur										
NB15 2.1A	UMD170728-434	4.5(2.5)	58	0.02887(85)	1.2022(23)	0.02504(42)	1.2	0.93(0.20)	0.52(0.46)	1.2025(23)
NB15 2.1B	UMD170728-445	63.0(3.0)	68	0.0493(11)	1.1951(25)	0.003395(55)	15	0.93(0.20)	4.30(0.12)	1.1975(25)
NB15-2.1-B2	UME190624-546	95.5(0.8)	84	0.06871(81)	1.1966(26)	0.001657(33)	41	0.93(0.20)	6.297(0.085)	1.2001(26)

^{a} Activity ratios determined at the University of Melbourne after Hellstrom (2003) and Drysdale et al. (2012)
^{b} Age in kyr before year of measurement (2016–2019), corrected for initial ^{230}Th using eqn. 1 of Hellstrom (2006) and the decay constants of Cheng et al. (2013)
^{c} Initial [^{234}U/^{238}U] calculated using corrected age
^{d} estimated initial [^{230}Th/^{232}Th] after Hellstrom (2006)
* sample discarded as outlier
2-σ uncertainties in brackets are of the last two significant figures presented

S5 Data of LOP analysis

In Tables S2, S3 and S4, the data of the LOP analysis are given. These data or simple calculations thereof were used to create Figures 3 to 7 in the manuscript.

Table S2. LOP data of flowstone samples.

Sample	C in ng/g	C in % of Σ8	S in ng/g	S in % of Σ8	V in ng/g	V in % of Σ8	C/V	S/V	Σ8 in ng/g
WP1	17.6±0.8	54.9	6.9±1.1	21.5	7.6±0.9	23.6	2.33±0.28	0.91±0.18	32.1
WP2	23.5±1.6	65.2	5.3±0.9	14.6	7.3±0.8	20.2	3.22±0.40	0.72±0.15	36.0
NB1	26.7±1.4	29.0	48.3±1.7	52.6	16.8±0.8	18.3	1.58±0.11	2.87±0.17	91.8
NB2	12.3±0.8	9.1	85.4±1.6	62.8	38.3±1.1	28.2	0.32±0.02	2.23±0.07	136.1
HC1	9.6±0.9	13.6	39.4±2.2	55.6	21.8±1.6	30.7	0.44±0.05	1.81±0.17	70.9
HC2	35.3±1.8	26.0	73.8±3.1	54.4	26.7±1.9	19.6	1.32±0.12	2.77±0.23	135.8
DC1	23.3±0.6	54.6	11.4±0.8	26.7	8.0±0.7	18.7	2.92±0.25	1.43±0.15	42.8
DC2	14.0±0.5	56.6	5.7±0.9	22.9	5.1±0.7	20.6	2.75±0.41	1.11±0.24	24.7

Table S3. LOP data of XAD samples.

Sample	C in ng/g	C in % of Σ8	S in ng/g	S in % of Σ8	V in ng/g	V in % of Σ8	C/V	S/V	Σ8 in ng/g
XAD-CC4	35.4±7.7	6.4	252.0±20.0	45.3	268.9±61.5	48.3	0.13±0.04	0.94±0.23	556
XAD-DC1	62.6±6.7	16.4	245.1±17.8	64.0	75.1±42.6	19.6	0.83±0.48	3.27±1.87	383
XAD-DC2	33.7±4.7	14.8	138.0±11.7	60.5	56.2±34.6	24.7	0.60±0.38	2.46±1.52	228
XAD-HC3	76.4±5.0	6.4	808.2±42.7	67.2	318.6±29.9	26.5	0.24±0.03	2.54±0.27	1203
XAD-HC4	134.7±8.9	3.5	2844.2±110.3	73.7	877.8±92.8	22.8	0.15±0.02	3.24±0.36	3857
XAD-HC5	41.0±4.6	6.0	507.3±24.5	73.7	139.9±16.0	20.3	0.29±0.05	3.63±0.45	688
XAD-WP1b	79.6±6.7	11.3	466.5±15.2	66.3	157.2±8.1	22.3	0.51±0.05	2.97±0.18	703
XAD-WP2	71.9±6.4	5.0	673.9±32.2	47.1	686.0±167.4	47.9	0.10±0.03	0.98±0.24	1432
XAD-WP3	55.8±5.6	8.8	368.5±21.9	58.4	206.8±24.0	32.8	0.27±0.04	1.78±0.23	631

Table S4. LOP data of soil samples. The sample without number gives the mean value of the respective subsamples 1 and 2.

Sample	C in ng/g	C in % of Σ8	S in ng/g	S in % of Σ8	V in ng/g	V in % of Σ8	C/V	S/V	Σ8 in ng/g
HC-LL-1	42099 ± 3185	0.3	7612898 ± 173922	58.1	5457133 ± 140850	41.6	0.008 ± 0.001	1.395 ± 0.048	13112130
HC-LL-2	85995 ± 5751	0.8	5179573 ± 280885	46.3	5927765 ± 287069	53.0	0.015 ± 0.001	0.874 ± 0.064	11193333
HC-LL	64047 ± 21948	0.5	6396236 ± 1216663	52.6	5692449 ± 235316	46.8	0.011 ± 0.003	1.134 ± 0.261	12152731
HC-O-1	5710 ± 407	0.2	1308053 ± 79057	40.8	1889054 ± 132349	59.0	0.003 ± 0.000	0.692 ± 0.064	3202817
HC-O-2	5784 ± 387	0.2	1388208 ± 53574	43.2	1816614 ± 53042	56.6	0.003 ± 0.000	0.764 ± 0.037	3210606
HC-O	5747 ± 37	0.2	1348131 ± 40077	42.0	1852834 ± 36220	57.8	0.003 ± 0.000	0.728 ± 0.036	3206712
HC-A-1	3418 ± 409	1.8	66147 ± 6758	35.0	119431 ± 6476	63.2	0.029 ± 0.004	0.554 ± 0.064	188995
HC-A-2	3168 ± 307	2.2	43143 ± 3108	29.9	98010 ± 3657	67.9	0.032 ± 0.003	0.440 ± 0.036	144321
HC-A	3293 ± 125	2.0	54645 ± 11502	32.8	108720 ± 10711	65.2	0.030 ± 0.002	0.497 ± 0.057	166658
NB-LL-1	49962 ± 3092	0.5	4024223 ± 160874	43.3	5218472 ± 148991	56.2	0.010 ± 0.001	0.771 ± 0.038	9292658
NB-LL-2	32211 ± 2642	0.3	6334970 ± 124043	56.0	4938845 ± 134087	43.7	0.007 ± 0.001	1.283 ± 0.043	11306026
NB-LL	41087 ± 8876	0.4	5179597 ± 1155374	50.3	5078659 ± 139814	49.3	0.008 ± 0.002	1.027 ± 0.256	10299342
NB-O-1	43476 ± 2871	0.8	1843128 ± 55771	35.7	3278336 ± 75716	63.5	0.013 ± 0.001	0.562 ± 0.021	5164940
NB-O-2	45689 ± 2395	1.0	1662910 ± 69360	36.1	2896181 ± 67000	62.9	0.016 ± 0.001	0.574 ± 0.027	4604780
NB-O	44582 ± 1107	0.9	1753019 ± 90109	35.9	3087259 ± 191078	63.2	0.015 ± 0.001	0.568 ± 0.006	4884860
NB-A-1	25211 ± 1548	0.6	2053946 ± 108664	46.3	2357578 ± 55638	53.1	0.011 ± 0.001	0.871 ± 0.050	4436735
NB-A-2	27878 ± 1583	0.6	1962094 ± 43932	45.0	2366376 ± 64978	54.3	0.012 ± 0.001	0.829 ± 0.029	4356348
NB-A	26544 ± 1333	0.6	2008020 ± 45926	45.7	2361977 ± 4399	53.7	0.011 ± 0.001	0.850 ± 0.021	4396542
WP-LL-1	23470 ± 9154	0.4	38624 ± 12842	0.6	6018255 ± 204881	99.0	0.004 ± 0.002	0.006 ± 0.002	6080348
WP-LL-2	32591 ± 1516	0.6	30324 ± 10915	0.5	5703594 ± 173781	98.9	0.006 ± 0.000	0.005 ± 0.002	5766509
WP-LL	28030 ± 4561	0.5	34474 ± 4150	0.6	5860925 ± 157330	98.9	0.005 ± 0.001	0.006 ± 0.001	5923429
WP-O-1	7445 ± 377	1.2	92375 ± 5975	15.5	497093 ± 29202	83.3	0.015 ± 0.001	0.186 ± 0.016	596913
WP-O-2	7156 ± 403	1.3	73999 ± 31172	13.7	458329 ± 23842	85.0	0.016 ± 0.001	0.161 ± 0.069	539485
WP-O	7300 ± 144	1.3	83187 ± 9188	14.6	477711 ± 19382	84.1	0.015 ± 0.000	0.174 ± 0.012	568199
WP-A-1	5829 ± 337	10.1	4871 ± 1270	8.4	47055 ± 3281	81.5	0.124 ± 0.011	0.104 ± 0.028	57756
WP-A-2	2458 ± 273	3.9	5620 ± 1333	9.0	54181 ± 1496	87.0	0.045 ± 0.005	0.104 ± 0.025	62259
WP-A	4143 ± 1685	6.9	5246 ± 375	8.7	50618 ± 3563	84.4	0.085 ± 0.039	0.104 ± 0.000	60007
LX-LL-1	67625 ± 2898	3.3	742912 ± 32603	36.4	1229330 ± 30899	60.3	0.055 ± 0.003	0.604 ± 0.031	2039866
LX-LL-2	108958 ± 4367	5.3	731190 ± 29851	35.4	1226499 ± 31854	59.3	0.089 ± 0.004	0.596 ± 0.029	2066647
LX-LL	88291 ± 20667	4.3	737051 ± 5861	35.9	1227914 ± 1415	59.8	0.072 ± 0.017	0.600 ± 0.004	2053256
LX-O-1	25636 ± 1315	1.3	659252 ± 39129	32.9	1318781 ± 49196	65.8	0.019 ± 0.001	0.500 ± 0.035	2003669
LX-O-2	10881 ± 517	0.6	599536 ± 43386	33.0	1205894 ± 61752	66.4	0.009 ± 0.001	0.497 ± 0.044	1816311
LX-O	18259 ± 7377	1.0	629394 ± 29858	33.0	1262337 ± 56444	66.1	0.014 ± 0.005	0.499 ± 0.001	1909990
LX-A-1	6970 ± 338	14.6	4346 ± 1576	9.1	36486 ± 1384	76.3	0.191 ± 0.012	0.119 ± 0.043	47801
LX-A-2	6764 ± 363	12.4	5672 ± 1597	10.4	42049 ± 1437	77.2	0.161 ± 0.010	0.135 ± 0.038	54485
LX-A	6867 ± 103	13.4	5009 ± 663	9.8	39267 ± 2782	76.8	0.176 ± 0.015	0.127 ± 0.008	51143

References

Cheng, H., Lawrence Edwards, R., Shen, C.-C., Polyak, V. J., Asmerom, Y., Woodhead, J., Hellstrom, J., Wang, Y., Kong, X., Spötl, C., Wang, X., and Calvin Alexander, E.: Improvements in ^{230}Th dating, ^{230}Th and ^{234}U half-life values, and U–Th isotopic measurements by multi-collector inductively coupled plasma mass spectrometry, Earth and Planetary Science Letters, 371-372, 82–91, https://doi.org/10.1016/j.epsl.2013.04.006, 2013.

Drysdale, R. N., Paul, B. T., Hellstrom, J. C., Couchoud, I., Greig, A., Bajo, P., Zanchetta, G., Isola, I., Spötl, C., Baneschi, I., Regattieri, E., and Woodhead, J. D.: Precise microsampling of poorly laminated speleothems for U-series dating, Quaternary Geochronology, 14, 38–47, https://doi.org/10.1016/j.quageo.2012.06.009, 2012.

Heidke, I., Scholz, D., and Hoffmann, T.: Quantification of lignin oxidation products as vegetation biomarkers in speleothems and cave drip water, Biogeosciences, 15, 5831–5845, https://doi.org/10.5194/bg-15-5831-2018, 2018.

Hellstrom, J.: Rapid and accurate U/Th dating using parallel ion-counting multi-collector ICP-MS, Journal of Analytical Atomic Spectrometry, 18, 1346, https://doi.org/10.1039/b308781f, 2003.

Hellstrom, J.: U–Th dating of speleothems with high initial ^{230}Th using stratigraphical constraint, Quaternary Geochronology, 1, 289–295, https://doi.org/10.1016/j.quageo.2007.01.004, 2006.

Hewitt, A. E.: New Zealand soil classification, vol. no. 1 of *Landcare Research science series, 1172-269X*, Manaaki Whenua Press, Lincoln N.Z., 3rd ed. edn., 2010.

Nava-Fernandez, C., Hartland, A., Gázquez, F., Kwiecien, O., Marwan, N., Fox, B., Hellstrom, J., Pearson, A., Ward, B., French, A., Hodell, D. A., Immenhauser, A., and Breitenbach, S. F. M.: Pacific climate reflected in Waipuna Cave drip water hydrochemistry, Hydrology and Earth System Sciences, 24, 3361–3380, https://doi.org/10.5194/hess-24-3361-2020, 2020.